A tale of two localizations: coexistence of flat bands and Anderson localization in a photonics-inspired amorphous system

Elizabeth J. Dresselhaus,[1, *] Alexander Avdoshkin,[1, 2, *] Zhetao Jia, Matteo Seclí,[3] Boubacar Kanté,[3, 4] and Joel E. Moore[1, 4]

[1]*Department of Physics, University of California, Berkeley, California 94720, USA*
[2]*Department of Physics, Massachusetts Institute of Technology, Cambridge, MA 02139, USA*
[3]*Department of Electrical Engineering and Computer Sciences,*
University of California, Berkeley, California 94720, USA
[4]*Materials Sciences Division, Lawrence Berkeley National Laboratory, 1 Cyclotron Road, Berkeley, California 94720, USA*
(Dated: April 29, 2024)

Emerging experimental platforms use amorphousness, a constrained form of disorder, to tailor meta-material properties. We study localization under this type of disorder in a class of $2D$ models generalizing recent experiments on photonic systems. We explore two kinds of localization that emerge in these models: Anderson localization by disorder, and the existence of compact, macroscopically degenerate localized states as in many crystalline flat bands. We find localization properties to depend on the symmetry class within a family of amorphized kagomé tight-binding models, set by a tunable synthetic magnetic field. The flat-band-like degeneracy innate to kagomé lattices survives under amorphousness without on-site disorder. This phenomenon arises from the cooperation between the structure of the compact localized states and the geometry of the amorphous graph. For particular values of the field, such states emerge in the amorphous system that were not present on the kagomé lattice in the same field. For generic states, the standard paradigm of Anderson localization is found to apply as expected for systems with particle-hole symmetry (class D), while a similar interpretation does not extend to our results in the general unitary case (class A). The structure of amorphous graphs, which arise in current photonics experiments, allows exact statements about flat-band-like states, including such states that only exist in amorphous systems, and demonstrates how the qualitative behavior of a disordered system can be tuned at fixed graph topology.

I. INTRODUCTION

Amorphous materials are defined by exhibiting local order in the absence of long-range order. They have traditionally been preferred in optical applications due to their isotropic properties and robustness, while still maintaining the necessary spectral gap [1]. More recently, engineered amorphousness has also been used in photonic meta-materials for similar reasons [2]. Conversely, in electronics, crystalline structures are favored because of their higher electron mobility. This difference fundamentally arises from the distinct spectral properties of amorphous versus periodic systems that share similar local structure. The primary variation lies in the eigenmodes, whereas the permitted energy levels are relatively unaffected.

In this work, we study the structure of amorphous spectra and corresponding wavefunctions to understand how amorphous systems behave in ways that are not typical for generic disordered systems. The absence of translational invariance in any disordered system poses a challenge: study of crystalline solids is to a high degree aided by Bloch's theorem which explains both the presence of band gaps and the extended nature of the wave functions. Solid-state physics has traditionally focused on perturbative disorder of a general form (typically, random on-site potential or hopping terms), but with small amplitude (weak disorder) [3]. Amorphous disorder, in contrast, is an example of strong disorder of a very special form that is non-perturbative. It can be thought of as a discrete hopping disorder that "rewires" the underlying connectivity graph of a system, but preserves the hopping amplitude. This property along with the absence of periodicity makes theoretical studies of amorphousness challenging.

We focus on an amorphous version of the kagomé lattice with a spatially uniform hopping phase and corresponding flux around closed loops of the underlying graph, analogous to a synthetic magnetic field. This model is realizable in resonator-array photonic devices [4] and has recently been studied by the present authors in this context [5]. Additionally, it is structurally similar to the commonly studied models giving an approximate description of solids such as amorphous silicon or silicon dioxide [6]. The model preserves local order: it is defined on an hourglass graph, see Fig. 1, i.e., one composed of corner-sharing triangles.

Rigorous results for amorphous systems are scarce, with the notable exception of the demonstrated persistence of a spectral gap in amorphous tetrahedral bonded semiconductors despite disorder [7, 8]. The robustness of the gap to amorphous disorder is markedly different from the case of random on-site disorder, where sharp crystalline bands broaden with increasingly strong disorder until the material eventually becomes a featureless insulator. In our work, we demonstrate and prove new exact results about the persistence of macroscopically degenerate states coming from compactly localized states in the presence of amorphous disorder. In a slight misappropriation of language, we refer to these persistent highly degenerate energy levels as "flat bands" even though there is no Brillouin zone; they are flat bands as a function of external fluxes through a torus [9]. Furthermore, quite remarkably, we show that flat bands exist in amorphous systems that have no analog in their crystalline counterparts. Flat bands are conducive to the formation of correlated states, such as superconductivity

[10], quantum spin liquids [11] and the fractional quantum hall effect [12], and our model offers an interesting playground for this exploration as well as novel thermodynamic and transport features that accompany a spike in the density of states.

There are two standard pathways to the formation of flat bands: compact localized states due to destructive interference of hopping paths on a geometrically frustrated lattice, such as the kagomé [13] or pyrochlore lattice [14], and the Landau-level-like mechanism leading to topologically nontrivial flat bands[15]. Both types of flat bands are generically destroyed by on-site and other traditionally studied forms of disorder. In the context of this work, we only encounter flat bands of the first type, which arise from compactly localized states.

The mentioned decreased electron mobility in non-crystalline materials comes from the localization of some eigenmodes in the spectrum and it has also been observed for our model [5]. This phenomena is known as Anderson localization [16]. In the case of on-site disorder, a comprehensive paradigm has been established through application of thoroughly developed analytic tools [17] and tests in numerical simulations [18]. In amorphous systems the fate of Anderson localization has been considered [19–23] but a systematic study has not yet been undertaken. We begin to address this issue in this work by considering a model of amorphousness relevant to experiments in photonics. In particular, we find that, in some symmetry classes, for our model even the qualitative features of localization seem distinct from the standard paradigm.

The rest of the work is organized as follows. In Sec. II we introduce the model, defined on a kagomé lattice, and explain how we construct amorphous structures that are locally identical to kagomé lattices. In Sec. III we explain why flat bands exist in some members of this family of model Hamiltonians and show how not only do these flat bands persist in the presence of amorphous disorder, there are in fact model Hamiltonians on amorphous structures that host flat bands which are absent in their periodic counterparts. We then turn to examining localization in the dispersive bands of our model. In Sec. IV we introduce a method to compute the effective localization length of eigenstates and adapt the method of energy level spacing distribution analysis to our amorphous systems. In Sec. IV A and IV B we compare the localization properties of model systems tuned to be in two different symmetry classes.

We discuss differences and challenges that this comparison raises to the conventional symmetry classification of localization in disordered systems.

II. MODEL

The model we consider is motivated by experiments in photonic metamaterials [4]. The experimental platform consists of a $2D$ array of photonic resonators, where nearest neighbors are coupled to each other through two sets of waveguides. When the arm lengths of the waveguides within each pair differ, photon dynamics in the system are described by a magnetic tight-binding Hamiltonian [4] (in first quantization):

$$H_0 = \sum_{\Delta_i} e^{i\phi}(|i_1\rangle\langle i_2| + |i_2\rangle\langle i_3| + |i_3\rangle\langle i_1|) + h.c., \quad (1)$$

where Δ_i is the ith triangle of the kagomé lattice. Sites are ordered i_1, i_2, i_3 as a counterclockwise path around each triangle. The effective magnetic field globally averages to zero but does not vanish locally for $\phi \neq 0$.

We can access three different Altland-Zirnbauer (AZ) symmetry classes [24] simply by tuning the hopping phase ϕ. At generic ϕ the system possesses neither chiral nor particle-hole nor time reversal symmetry (AZ symmetry class A). Time reversal symmetry is preserved only when $\phi = 0, \pi$ (AZ symmetry class AI). When $\phi = \pi/2$, the Hamiltonian has particle hole symmetry under complex conjugation $H_0^* = -H_0$ and falls into AZ class D.

We will first consider the model of Eq. (1) on a (periodic) kagomé lattice. In the amorphous case, we define the model on graphs created by kagomization (explained in the next section) and refer to the analogous entities as amorphous systems. We note that this model is experimentally relevant at finite system size - photonic systems in experiments can have size $L \sim 100$, where L denotes the number of resonators per row.

A. Amorphous Model

We adapt the amorphous graphs we used in [5]: these graphs resemble kagomé lattices locally in that every vertex has coordination number $z = 4$ and is the center of a pair of corner-sharing triangles, however the graphs lack long range order and contain faces other than triangles and hexagons. Some experimental realizations of photonics systems, including the experiments in our previous work, require equal bond length between all connected sites. We relax this restriction in order to have a simple process of generating graphs that will be easily reproducible.

Beginning with an uncorrelated set of L_0^2 points in an $L_0 \times L_0$ region we use kagomization [25] to generate a graph with the short range order defined above but no long range order. This process can be consistently done for any system size L_0 which is necessary for extrapolating the results to the thermodynamic limit, see as in Sec. IV. The kagomization procedure is explained in Fig. 1: we first construct a Voronoi diagram from the uncorrelated set of points, and then generate triangles around each Voronoi vertex by connecting the midpoints of all Voronoi edges emanating from the vertex. These triangles form a kagomized graph with $S \sim 6L_0^2$ sites. We define the system size as $L = \sqrt{S}$. To implement this graph with periodic boundary conditions, we perform the same procedure for a random point set on a two-dimensional torus.

Kagomizations of Voroni graphs consist of corner-sharing triangles: this makes them a special type of hourglass graph. Some properties of these emerging hourglass graphs can be conveniently understood by considering the corresponding Delaunay triangulation, the dual graph of the Voronoi graph. Triangulation graphs are in one-to-one correspondence with hourglass graphs. At the same time, not all triangulations can
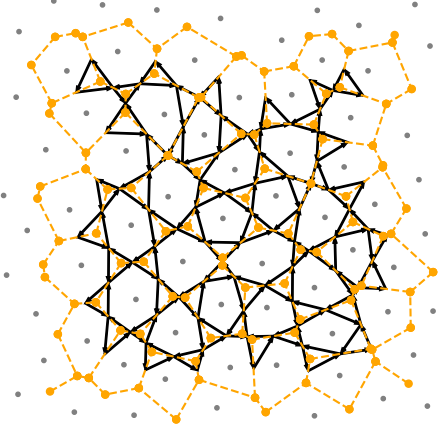
FIG. 1. Kagomization starts with a random, uncorrelated set of points (grey). Next, we generate the Voronoi diagram for this point set (orange) and then connect the midpoints on each edge to the neighboring edge midpoints to form the corresponding kagomized graph (black).

be realized as Delaunay triangulation graphs [26] and thus not all hourglass graphs will be generated by the procedure described in the previous paragraphs.

Any hourglass graph can be generated by a series of local updates to graph connectivity starting from the kagomé lattice. The local updates consist in restructuring a pair of adjacent triangles which correspond to diagonal flips [27] of the dual triangulation. The ability to construct an arbitrary graph in this way follows from the proven analogous result for triangulation graphs [28, 29]. Thus, considering all hourglass graphs gives the intriguing possibility to introduce amorphousness in a perturbative way. The simulation results in the next section pertain to hourglass graphs from kagomization, however, the exact results and arguments apply to any hourglass graph.

To write the model of Eq. (1) on a amorphous graph, we must be careful to only define hoppings around triangles that belonged to the original kagomé lattice. We refer to triangles of an amorphous graph that belonged to the original kagomé lattice as primitive triangles, and any cycles on the graph formed by connected primitive triangles as secondary polygons. On the kagomé lattice, all secondary polygons are hexagons, whereas on amorphous kagomized graphs, secondary polygons consist of N-sided polygons where $N = 3, 4, 5, 6, \cdots$. Writing our model on secondary triangles will give incorrect hopping terms. Thus, we define Eq. 1 on an amorphous graph by summing over all *primitive* triangles Δ_i of the graph. Numerically, this distinction is accomplished by writing the Hamiltonian from hoppings around the Voronoi vertices that give rise to a given kagomized graph.

III. COMPACTLY LOCALIZED FLAT BAND STATES IN AMORPHOUS MODEL

The model on a kagomé lattice gives rise to three energy bands in momentum space, which are gapped or ungapped depending on the choice of ϕ. A single flat band is present when $\phi = \ell\pi/6$ for integer ℓ. The degeneracy is at most $S/3+1$, where $S/3$ corresponds to the number of secondary hexagons in the graph.

The amorphous graph does not consist of only primitive triangles and hexagons. However, as in the kagomé lattice, every graph edge is a side of a triangle, and every vertex of the graph is tetravalent. Based on these observations, we show in App. A that flat band states always occur at energy $E_{fl} = 2\cos(3\phi + \pi)$. Below we describe in detail the structure of flat band states in amorphous systems for $\phi = 0$, and outline how this analysis can be generalized to $\phi = \ell\pi/6$. Additionally, we find that for other commensurate values of ϕ flat bands are only present in amorphous systems, not their kagomé lattice counterparts.

A. Robustness of flat bands to amorphousness in absence of field

In the kagomé lattice at $\phi = 0$, the local value (non-normalized) of a given flat band state $|\psi_{fl}\rangle$ alternates as ± 1 around a single hexagon and vanishes elsewhere, see Fig. 2 (a). When the Hamiltonian acts on $|\psi_{fl}\rangle$, destructive interference on each site neighboring the hexagon prevents this state from dispersing outside of the hexagon. This flat band state has degeneracy $S/3 + 1$.

We conjecture and prove in App. A that a spanning set of all flat band states on an amorphous graph for $\phi = 0$ is given by two types of states. Type-I are defined by the following conditions:

1. The state resides on a closed loop of even length.

2. This loop incorporates an even number of vertices of each primitive triangle, which is equivalent to the loop being non-intersecting

3. The state has (un-normalized) amplitudes ± 1 which alternate along the loop.

An example of a Type-I flat band state localized around a pentagon-septagon pair is shown in Fig. 2(b). Note that the wavefunction on the central site of this loop vanishes and that the action of the Hamiltonian on this state leads to destructive interference on this central site and all sites immediately neighboring the combined polygon. Type-I states can also reside on non-contractible loops of the torus.

Type-II states consist of pairs of non-adjacent odd-length secondary polygons that satisfy the following conditions:

1. The state resides on a combination of two non-adjacent closed loops connected by a path

2. The state has (un-normalized) amplitudes ±1 which alternate around the loops, but necessarily leaves two adjacent sites with the same sign, giving each loop a net sign

3. The connecting path must start at the third vertex of the primitive triangle that contains two adjacent sites with the same sign on one polygon, and end at the analogous vertex of the other polygon. The state on this path has (un-normalized) alternating amplitudes ±2

We refer to the connecting path as a "Dirac string" in analogy to electromagnetism where a Dirac string connects two magnetic monopoles. The Dirac string is necessary for a Type-II state to be an eigenstate of Eqn. 1 on an amorphous graph. In fact, the Dirac strings appear exclusively in flat band states on amorphous graphs of our model system! An example of a Type-II state is shown in Fig. 3.

Numerical investigations find that the span of the set of Type-I and Type-II flat band states is *exactly* one third of the number of sites S in the graph. We also prove this result rigorously in App. A.

B. Robustness of flat bands to amorphousness at non-zero field

For $\phi = \frac{\ell}{6}\pi$, where ℓ is an integer, we similarly observe the persistence of a macroscopically degenerate levels (flat bands) in numerical simulations of amorphous systems.

Analogous to the previous subsection, one can construct a macroscopic number of flat band states that generalize the flat band states localized on hexagons on the kagomé lattice. We see that some flat band states reside on combinations of multiple polygons in these amorphous graphs. To define these states, we employ a ϕ-dependent integer p, whose ℓ-dependence is explained in App. A, for example $\phi = \pi/6, \pi/3, \pi/2$ corresponds to $p = 3, 6, 1$. To extend the conditions for Type-I flat band states to general p, we add p-dependence to conditions $1, 3$: (1) flat band states must reside on loops whose length is divisible by p ($p = 1$ implies any loop is valid) (3) the amplitudes are the p-th roots of unity, taken sequentially around the unit circle in the complex plane. For $\phi \neq 0$ it is also important to note that graphs become directed, and all loops that host flat band states must respect the orientation of the edges.

Remarkably, for $p = 1, 2, 6$ which correspond to $\phi = \pi/2, 0, \pi/3$, we see that the fraction of all eigenstates that are in the flat band remains $1/3$ even on the amorphous graphs. In general we do not expect this to be the case. For example in Table I we see that for $\phi = \pi/6$, the fraction of flat band states never exceeds $1/16$ in our simulations. Additionally, we observe that this fraction varies appreciably from realization to realization for most values of ϕ, see Table I. The reasoning for why this does not occur for $p = 2$ was explained in the previous subsection; the case $\phi = \pi/2$ ($p = 1$) can also be easily understood. The flat band state in this case does not alternate ±1 around a polygon but is in fact uniform. This simple structure of the flat band states ensures compatibility with all secondary polygons in the graph: every secondary n-gon in an amorphous system supports a uniform localized flat
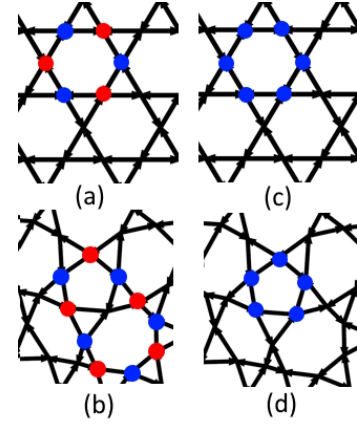

FIG. 2. Figures on left side represent a flat band state at $\phi = 0$; figures on right side represent a flat band state at $\phi = \pi/2$. (a) Flat band eigenstate alternates between +1 (blue circles) and −1 (red circles) around the hexagon and is zero-valued outside. (b) Flat band eigenstate of an amorphous kagomized system wraps around a pentagon-septagon combination such that the state's sign can still alternate between circumferential sites. (c) At $\phi = \pi/2$ the flat band state has the same phase at every site surrounding a hexagon. (d) Since the state's sign is constant around a polygon, the pictured flat band state localized around a pentagon in an amorphous kagomized system is an eigenstate for $\phi = \pi/2$.
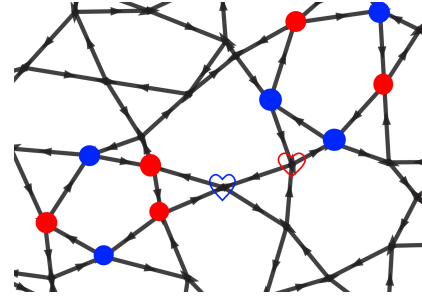

FIG. 3. Example of a flat band state at $\phi = 0$ that combines two *non-adjacent* polygons of odd length. The flat band eigenstate alternates between +1 (blue circles) and −1 (red circles), but leaves a net sign around each pentagon. While the compact localized state around each pentagon individually could not be an eigenstate, a "Dirac string" of +2 (blue heart) and −2 (red heart) connects the pentagons resulting in a flat band eigenstate.

band state surrounding it, see Fig. 2d. We believe an analysis similar to the previous subsection can be performed in these cases except that one would need to consider directed graphs. We leave this for future work.

C. Flat bands unique to amorphous systems

On the kagomé lattice, secondary hexagons cannot support localized eigenstates when p does not divide 6. However, amorphous graphs contain secondary polygons of various sizes, e.g. pentagons and septagons. Localized states around these polygons become possible through appropriately tuning ϕ to $\phi = \ell\pi/p - \pi/2$ for integer ℓ. This result can be derived

ϕ	kagomé lattice	amorphous system
0	S/3 + 1	S/3
$\pi/6$	S/3	$\leq$ S/16
$\pi/3$	S/3 + 1	S/3
$\pi/2$	S/3	$\lesssim$ S/3
$3\pi/8$	0	$\leq$ S/16
$3\pi/4$	0	$\leq$ S/8
$11\pi/10$	0	$\leq$ S/6

TABLE I. Numerical results (from 50 simulations of amorphous systems with $S = 48$) of flat band degeneracy for a subset of values of ϕ that give flat bands. Simulation results are shown for when the underlying graph of the system is a kagomé lattice or amorphous graph. Note that the number of flat band states can depend on the realization of amorphous disorder, in which case we provide an upper bound.

FIG. 5. Example of a localized state on an amorphous analog of the Lieb lattice. In the Lieb lattice, states can exist both at vertices of the graph as well as at midpoints of the graph edges, denoted by X in the figure. Blue (red) X denote non-normalized state amplitude $+1(-1)$ whereas white circles at the vertices and black Xs denote no state amplitude.

D. Other lattices

Besides the kagomé lattice, there are multiple other lattices that can support flat bands [31]. We expect that the fate of flat bands in the amorphous versions of these lattices will be similar to what we described for the kagomé case. As an illustration in Fig. 5, we show how localized states can persist in the amorphous version of the Lieb lattice. Other lattices that we believe will host flat band states in the amorphous form include the star lattice and dice lattice.

We will now focus on the dispersive bands of our model which, in the amorphous case, exhibit a distinct type of localized states that we refer to as Anderson-like localized states.
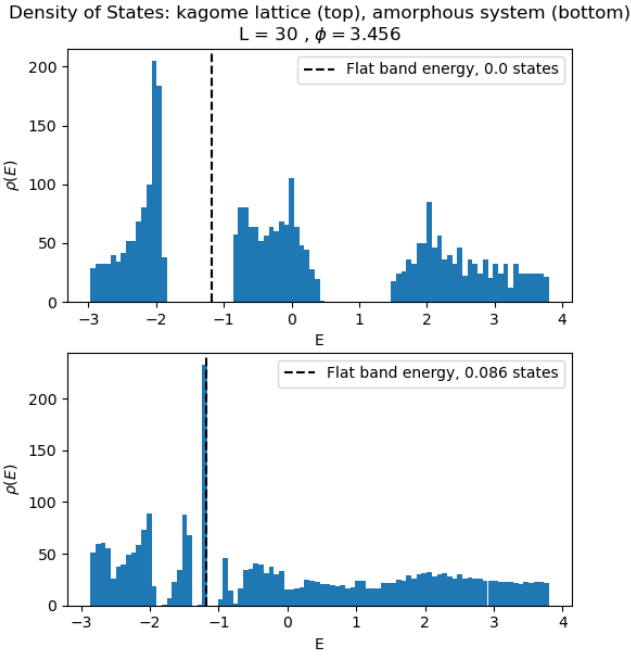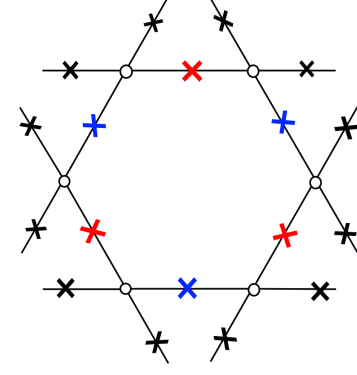

FIG. 4. Example of a case where a flat band exists in the amorphous system but *not* in the kagomé lattice system. For $\phi = 11\pi/10$, a flat band emerges in the amorphous system in the gap of the kagomé lattice. This flat band contains .086 of the total states of the system, unlike the 1/3 typically observed in flat bands in these systems. We hypothesize that these flat band states are hosted on pentagons.

from the results of App. A. We conjecture that at these values of ϕ, flat bands that were not present in the kagomé lattice will appear in amorphous systems! In Fig. 4, we illustrate it for the case $\phi = 11\pi/10$, corresponding to $p = 5$ (states localized around pentagons).

We note that these flat bands are expected to be topologically trivial. In 2D, it has been proven that topologically nontrivial flat bands can only exist if hopping is non-local[30], which is not the case in our model. Though the proof was done for periodic systems, we expect a similar result would apply in our case due to the local nature of most states in the flat band.

IV. ANDERSON-LIKE LOCALIZATION IN AMORPHOUS SYSTEMS

In a previous work including the authors of this study [5], we observed localization in the dispersive bands of amorphous systems in class D. The localization of states was dependent on their eigenenergy, with energy regions in the band tails giving rise to localized states. In this work, we confirm this observation by adapting two methods previously used to study localization: effective localization-length spectra and nearest energy level spacings. We then compare our results in class D (Sec. IV A) to class A, accessed by tuning ϕ (Sec. IV B).

We refer to the localization we observe as "Anderson-like" to distinguish it from true Anderson localization. Anderson localization is defined by states whose magnitude decays from a well-defined center as $|\psi|^2 \sim e^{-r/\xi}$ where r is the distance from the center and ξ is the localization length [32]. In Anderson-like localized states, the state can be localized about multiple centers, but still decays rapidly away from each center. Anderson-like localized states were previously observed in amorphous systems hosted on Voronoi graphs [19]. To detect localization of a state ψ, we calculate its inverse participation

ratio I_2 (IPR), defined as

$$I_2 = \sum_{i=1}^{S} |\psi_i|^4 \qquad (2)$$

Where S is the number of sites on the graph and ψ is normalized. We define an effective localization length $\tilde{\xi} = \frac{1}{\sqrt{I_2}}$. While inequivalent to the true localization length ξ, best approximated using the smallest quasi-1d Lyapunov exponent [33], the effective localization length is well suited to describing localization in amorphous systems for systems sufficiently small to be efficiently diagonalized.

We also analyze nearest-level spacings distributions. The set of nearest level spacings ΔE for a system is defined as the absolute difference between all nearest neighbors in an ordered set of the system's eigenenergies. To define a distribution of the spacings, spacings are first normalized by the mean spacing to define $s = \Delta E / < \Delta E >$. In the limit of infinite system size, nearest-level spacings distributions in Anderson model disordered systems have been shown to fit either a Poisson law, $P_P(s) = 1/\delta e^{-(s/\delta)}$, or the Wigner surmise for the orthogonal class ($\beta = 1$), $P_O(s) = \frac{\pi}{2\delta} s e^{-(\pi/4s^2)}$ or a hybrid function, [34]. These three cases correspond to systems with only localized states, only delocalized (metallic) states, and systems at the metal-insulator transition.

In the 2D Anderson model all eigenstates of a system are localized for arbitrarily small onsite disorder strength [3]. For large onsite disorder the 3D Anderson model also becomes insulating at all energies, however for sufficiently small onsite disorder, energy eigenstates at low energies are delocalized and energy eigenstates at higher energies are localized, separated by a mobility edge [35]. We observe that amorphous systems qualitatively resemble the 3D Anderson model with weak disorder: the states can be either localized and/or delocalized, depending on which energy we probe.

An important difference from the Anderson model is that, for $\phi \neq 0$, systems break time reversal symmetry. Thus in our analysis we use the Wigner surmise for the unitary class (class A), $\beta = 2$, $P_W(s) = \frac{32}{\pi^2} s^2 e^{-4s^2/\pi}$ [36]. The Wigner surmise for class D coincides with that of class A for states at sufficiently high energy [37]. We define subsets of all eigenstates using cutoff $\tilde{\xi}/L < 1/3$ to approximate which states are localized, shown in Fig. 6, 8. We examine the largest system size only. For each amorphous system of this size, we choose all energies within a range R. Then we select energies $E_{i,R}$ in this range and find the nearest level spacings $\Delta E_{i,R}$ and normalize this set by its mean. We then compute a histogram for the normalized spacings $\Delta E_{i,R}$. Using the same histogram bins, we repeat this procedure for all realizations, then find the average value and error bar for each bin. For each range R, we fit a Poisson distribution and a Wigner distribution and then compute the p-value from the Kolmogorov-Smirnoff statistic p for each fit. A large value $p \sim 1$ indicates that the data is likely to have come from this type of distribution whereas $p \sim 0$ indicates that the data comes from a different distribution. Results of these analyses are shown in Fig. 7, 9.

A. Anderson-like localization in class D

We start with a brief overview of the spectral properties of the periodic (kagomé lattice) system in class D ($\phi = \pi/2$). This system has three gapped energy bands in momentum space: a flat band at $E = 0$ sandwiched by two particle-hole symmetric bands $E_\pm$. We focus on the highest energy band throughout all following analyses. The top band spans $E = (\sqrt{3}, 2\sqrt{3})$ and has a Lifshitz transition at $E = 2$. Due to momentum space degeneracy, $I_2(E_+)$ is multi-valued and $\tilde{\xi}(E)$ forms an envelope. This envelope is strongly centered around $\tilde{\xi}(E) \sim O(1)$ for all energies, consistent with the delocalized nature of these eigenstates that we expect because of translation invariance.

Amorphous class D systems retain the gapped three-band structure of their kagomé counterparts. The flat band is protected from amorphousness by particle-hole symmetry as well as the arguments outlined in Sec. III. Numerically, we generate and diagonalize the Hamiltonian of amorphous systems of size L_0 ranging from $L_0 = 40$ to $L_0 = 100$ and calculate I_2 for all eigenstates. To focus on bulk properties, we apply periodic boundary conditions in both directions for all calculations, unlike in [5] where we used open boundary conditions.

The effective localization spectrum for a large class D amorphous system ($L_0 = 100$) is shown in Fig. 6. The density of states of the bulk band extends into the bandgap of the kagomé lattice but the amorphous disorder is not sufficiently strong to close the gap. Most states in the amorphousness-induced tail, with energies $E < \sqrt{3}$, have suppressed effective localization length. However, not all states with $\tilde{\xi} << L$ are in the tails: even in large systems, some states deep in the metallic (delocalized) region of the bulk are relatively localized. In fact, effective localization length $\tilde{\xi}$ can vary considerably between states that are close in energy, forming an envelope structure similar to that observed in the kagomé lattice. The envelope structure complicates defining a mobility edge in these systems. To approximate a mobility edge, we define energy ranges such that the effective localization length probability distribution can be split into two distinct regions, the "localized" states, shown in blue in Fig. 6 and "delocalized" states shown in red, with minimal overlap. All eigenstates outside of these categories we categorize as "metal insulator transition" states (purple). Setting cutoff $\tilde{\xi}/L < 1/3$ for classifying localized states coincides with this analysis.

Considering a single realization of amorphousness at experimentally relevant sizes without scaling illustrates the complexity of localization in these amorphous systems. Scaling-based evidence for localization from amorphousness was previously shown in [5] where we averaged I_2 over multiple realizations of amorphousness for various system sizes. We observed that I_2 for eigenstates in the bulk band tails remains approximately constant while increasing system size. While numerical data for only a single system size is presented here, additional data suggests that the approximate mobility edge location is independent of system size for systems from $L = 20$ to $L = 100$.

The nearest-level-spacings of states assigned to the localized energy range fit a Poisson law well. The spacings of states assigned to the delocalized energy range do not come from a
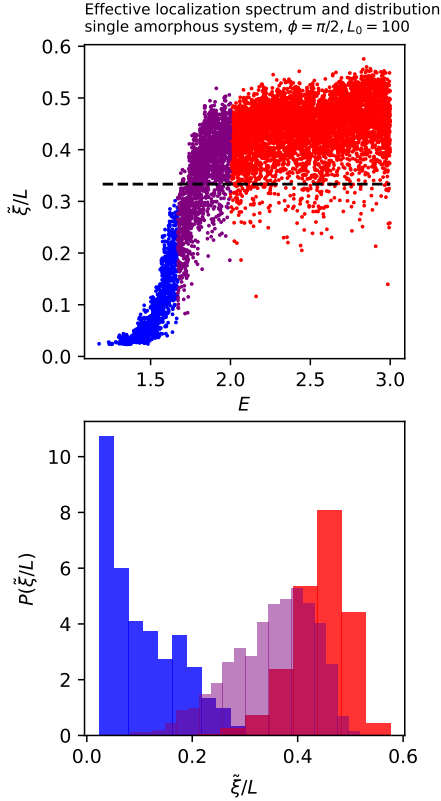
Effective localization spectrum and distribution
single amorphous system, $\phi = \pi/2, L_0 = 100$

Nearest level-spacing distribution for
localized states E = (1.2, 1.67)
for amorphous system, $\phi = \pi/2, L_0 = 100$

Nearest level-spacing distribution for
delocalized states E = (2, 3)
for amorphous system, $\phi = \pi/2, L_0 = 100$

FIG. 6. Top: Scatter plot of the energy of every eigenstate in the highest energy band of an $L_0 = 100$ amorphous system and its effective localization length. States are separated into three energy ranges, corresponding to localized (blue), metal-insulator-transition (purple) and delocalized (red). Bottom: States classified as localized (red) have nonzero probability $P(\tilde{\xi}/L)$ for $\tilde{\xi}/L < 1/3$. The energy range for delocalized states is set such that the delocalized states' (red) probabilities' non-zero range has minimal overlap with the localized states' range. All states in-between are classified as metal insulator transition states, whose distribution $P(\tilde{\xi}/L)$ is shown in purple.

Poisson law distribution, nor do they fit the Wigner distribution with a high degree of certainty. This inconclusivity is likely due to the persistence of localized states deep in the metallic phase, as shown in Fig. 6.

B. Anderson-like localization in Class A

In the following, we repeat the analysis of Sec. IV A for a system of Eq. (1) for a system with broken particle hole symmetry: in AZ class A. For subsequent calculations we set $\phi = 4\pi/9$, such that the bulk remains gapped, see Fig. 8. The middle band has now broadened and the surrounding bands are no longer particle-hole symmetric. The upper band, however, retains qualitatively similar features to the class D case. In class A, we also observe a completely delocalized state at $E = -.695$, see Fig. 8. This completely delocalized state,
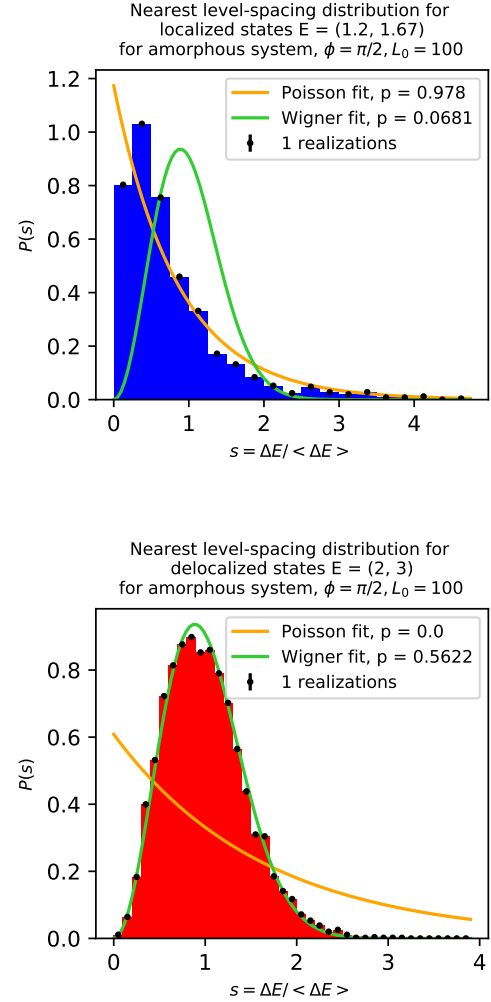
FIG. 7. Top: Nearest level-spacings distributions of states in the localized energy range, averaged over 6 realizations of amorphous systems of size $L_0 = 100$. Error bars are in black for each bin. Best-fits for a Poisson law distribution and Wigner distribution are shown in orange and green, respectively. The distribution is likely to have come from the same distribution as the Poisson law. Bottom: Nearest level-spacings distributions of states in the delocalized energy range. The distribution is unlikely to have come from the same distribution as the Poisson law and likely to have come from the Wigner surmise.

with equal amplitude on each site, is an eigenstate of Eq. (1) with energy $E = -4\cos\phi$. We also observe this state in App. B. The existence of this completely delocalized eigenstate is a consequence of the local on-site Hamiltonian appearing the same on every site of the system. This state did not appear in the class D analysis because it occurs at the same energy as the flat band states and can be written as a superposition of flat band states. In Fig. 9 we repeat the level spacings analysis of the previous section of subsets of this upper band and find qualitatively similar results to the analysis in class D.

For context, we review current thinking about which properties are universal in generically disordered systems, using class A systems as an example. This model can be mapped
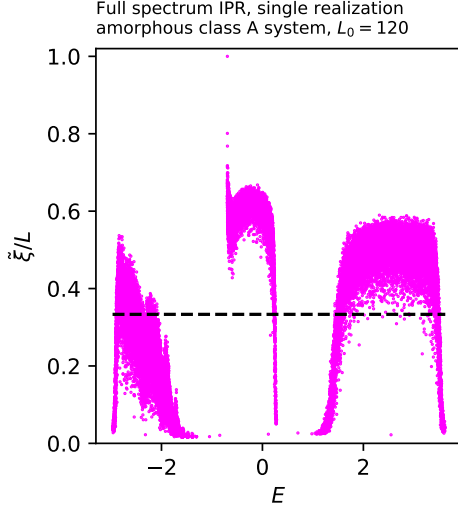
FIG. 8. Scatter plot of the energy of every eigenstate of $L_0 = 120$ amorphous system with $\phi = 4\pi/9$, symmetry class A. The highest energy band localization is similar to highest energy band (and its particle-hole-symmetric partner) in class D. However, the flat band has broadened and the lowest band appears to have mostly localized states, unlike in class D. A fully delocalized state with $\tilde{\xi}/L = 1$ exists at $E = -4\cos(4\pi/9)$.

to a $2D$ disordered Dirac fermion picture. A long-standing conjecture suggested that the localization-delocalization transition of $2D$ disordered Dirac fermions is controlled by the same fixed point as the integer quantum Hall transition of ordinary fermions[38]. In the integer quantum Hall transition, a class A system, the localization length of states in a bulk band diverges at the critical energy E_c as $\xi \sim |E - E_c|^{-\nu}$ [39]. Thus in class A disordered Dirac fermions, we expect states in the bulk bands to be fully localized even for infinitesimally weak disorder except for a single delocalized state in the center of the bulk band. Numerical results have confirmed this fact for onsite disorder in class A [40], even if it is not absolutely clear that the exponent ν is the same between Dirac and quadratic fermions in a magnetic field. We cannot interpret our results for amorphous disorder in class A within this basic picture due to the extended range of delocalized states shown in Fig. 9. This suggests that the amorphous nature of the system may require an expansion of the symmetry classification to include new types of localization phenomena.

We stress that we cannot strictly rule out the possibility that an extended range of delocalized states for amorphous class A systems is a finite size effect. However, this observation certainly calls for future work, both numerically and analytically, to determine whether amorphous disorder can be fit into the AZ symmetry classification. We also note that the system sizes we simulate are on the scale of experimental topological photonics systems, thus even if delocalized states only appear so as a result of finite size, they may be effectively metallic for applications.
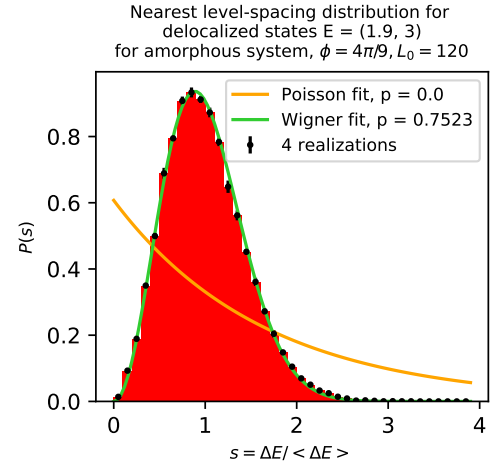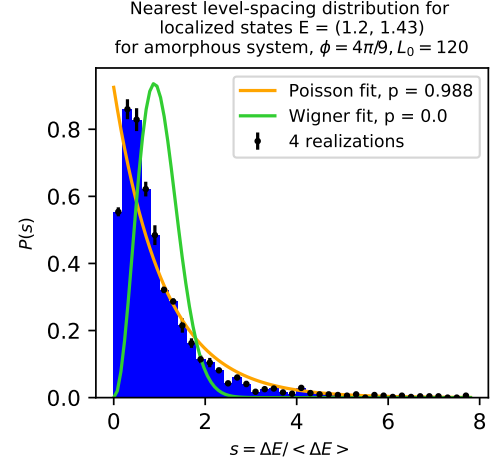

FIG. 9. Top: Nearest level-spacings distributions of states in the localized energy range, averaged over 43 realizations of amorphous systems of size $L_0 = 120$ with $\phi = 4\pi/9$. Error bars are in black for each bin. Best-fits for a Poisson law distribution and Wigner distribution are shown in orange and green, respectively. The distribution was drawn from the same distribution as the Poisson law. Bottom: Nearest level-spacings distributions of states in the delocalized energy range. The distribution was drawn from the same distribution as the Wigner surmise.

V. CONCLUSION

In this work, we explored two types of localization in an amorphous topological-photonics-inspired model: compact localized states in flat bands and Anderson-like localized states. This model can access different physics and symmetry classes through tuning effective magnetic flux ϕ.

We show that flat bands appearing in the kagomé lattice model for $\phi = n\pi/6$, which are destroyed by onsite disorder, persist in the presence of amorphous disorder. This work opens up the study of features such as band-touching between flat bands and dispersive bands [41] in amorphous systems. We also show that partial flat bands occur in amorphous systems

at some values of ϕ which are *absent* in their kagomé lattice counterparts. In these flat bands unique to amorphous systems, it is possible to tune the number of flat band states by modifying the structure of the underlying graph, which may be useful for some applications.

Beyond these localized flat band states, we also demonstrate Anderson-like localization that is induced by amorphousness. To study these localization properties, we use and adapt two methods: inverse-participation-ratio (IPR) calculations and energy-level-spacings analysis. We find that this type of localization occurs in the symmetry classes we would expect from studies of onsite disordered systems, however, the observed extent of the spectrum which is localized, particularly in symmetry class A, differs from the Anderson paradigm of localization.

For context for our results, we point out the work by Puschmann who considered random $2D$ Voronoi Delaunay lattices with out-of-plane uniform magnetic field (class A) and found quantum Hall edge states with localized bulk modes. This work also presents evidence that the critical properties of this model agree with models in class A with only onsite disorder [19]. Although this model is in class A, the implementation of amorphous disorder and magnetic field differed. This might mean the implementation of amorphousness is crucial for Anderson localization.

For additional context, one can also consider the Aubry-André (AA) model, a 1D lattice with quasi-periodically modulated hoppings. Although universality predicts that all state must localize for an arbitrary weak disorder in the relevant symmetry class, in the AA model localization happens at a finite value of the modulation amplitude. This result suggests that in order to modify universality, disorder must be constrained to an extreme degree (there are only two global parameters in the case of the AA model, so arguably "disorder" is no longer even the right word). Here is an important distinction between our observation of the modification of universality and the analogous case in the AA model: our example exhibits refined universality in a model where the randomness still has an extensive number of degrees of freedom.

The methods we use to study localization in amorphous systems may also be applicable to studying newly-discovered fractional states in amorphous Chern insulators [42] and amorphous chiral spin liquids [43]. We also emphasize that our model system offers an approach to study introducing amorphousness perturbatively through combining local diagonal flips in the dual graph of a system.

This work also has application to the study of phases and universal behavior in two-dimensional disordered topological superconductors in symmetry class D. Such superconductors show metal-insulator transitions with onsite disorder [44] and non-linear sigma model RG analysis predicts quasiparticle localization [45]. While a recent study claims that amorphous Chern insulators in class D have non-universal critical behavior [46], more research is needed to verify these claims. Here we have proposed an alternate microscopic model, with the ability to tune the degree of amorphousness without destroying local order. This will be a useful tool to further study metal-insulator transitions in both topological superconductors and in amorphous Chern insulators in class D.

This work raises a multitude of questions that need further exploration, about (1) flat bands, (2) the fate of periodic band structures when the underlying graph is made amorphous and (3) Anderson-like localization in the thermodynamic limit. We outline these areas for continued investigation below.

- What determines the degeneracy of a flat band? In App. A we derive the degeneracy for $\phi = 0, \pi/2$ for both kagomé and amorphous systems. However, as seen in Table I, numerical simulations show that other values of ϕ have different flat band degeneracies for which our derivation is not sufficient.

- Why do some bands of periodic band structures survive while others do not when the underlying structure is made amorphous? For example, in our model systems we see that the class D three-band structure from the periodic case is preserved (with tails extending into the periodic system bandgap as in Fig. 6). However, for $\phi = 11\pi/10$ the density of states plots in Fig. 4 indicate that the lowest energy band retains its qualitative character, two additional bands (one flat) are created in the bandgap, and the highest two energy bands blur together. Further work is needed to explain why (a) some bands are minimally affected by the system becoming amorphous and (b) this effect depends on ϕ.

- How do we understand the envelope structure observed in the effective localization spectrum in amorphous systems? The envelope does not appear to shrink with increasing system size, unlike in numerical simulations of onsite disorder. Furthermore, amorphous systems violate Mott's argument: localized and delocalized states can exist at arbitrarily close energy spacing. We hypothesize that this is due to the discrete and constrained nature of amorphous disorder. Extending Mott's argument to amorphous systems is an interesting avenue for further analytical and numerical exploration.

- How do we identify universality classes of amorphous localization phase transitions? What aspects of amorphous disorder become relevant to such a classification?
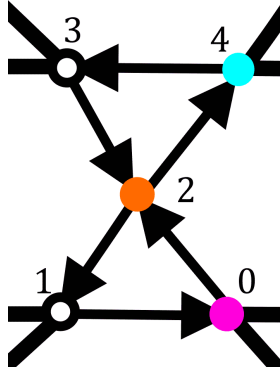
VI. ACKNOWLEDGEMENTS

FIG. 10. A flat band state on a segment of an n-gon. The flat band state is valued $e^{i\alpha}$ (pink circle), $e^{i\beta}$ (orange circle), and $e^{i\gamma}$ (teal circle) on sites inside the polygon, and vanishes outside the polygon (white circles). The Hamiltonian, particularly the choice of ϕ, determines the relative phases of the state around the polygon, and the graph geometry determines whether the system hosts a flat band eigenstate at this value of ϕ.

Appendix A: Flat Band calculations

1. Flat band structure

We can construct these flat band states for a Hamiltonian of general phase by considering the action of the Hamiltonian on a flat band state defined around a single section of an $n-$gon. In Fig. 10 we define a basis such that even-indexed sites form a polygon and odd sites are connected to the polygon. Note that this construction applies to any polygon of $n \geq 3$. Based on this diagram, we formulate an ansatz for a (non-normalized) flat band state as $|\psi_{fl}\rangle = e^{i\alpha}|0\rangle + e^{i\beta}|2\rangle + e^{i\gamma}|4\rangle + \cdots$ where the state vanishes on odd-index sites in the basis and exists on even-indexed sites of the $n-$gon peripheral to this diagram. Action of the Hamiltonian gives:

$$H|\psi_{fl}\rangle = (e^{i\alpha}e^{-i\phi} + e^{i\beta}e^{i\phi})|1\rangle + $$
$$(e^{i\alpha}e^{i\phi} + e^{i\gamma}e^{-i\phi})|2\rangle + (e^{i\gamma}e^{i\phi} + e^{i\beta}e^{-i\phi})|3\rangle + \cdots$$

For $|\psi_{fl}\rangle$ to be an eigenstate:

$$\Delta\phi = \alpha - \beta = \beta - \gamma \mod 2\pi = 2\phi + \pi \mod 2\pi \quad \text{(A1)}$$
$$e^{i\alpha}e^{i\phi} + e^{i\gamma}e^{-i\phi} = E_{fl}e^{i\beta} \quad \text{(A2)}$$

Combining the above equations gives:

$$E_{fl} = 2\cos(3\phi + \pi) \quad \text{(A3)}$$

This analysis suggests that, in principle, a flat band state could exist at any value of ϕ in our model systems. However, the geometry of the underlying graphs of these systems restricts the values of ϕ at which we see flat bands. States can only be eigenstates of the Hamiltonian if they live on n-gons where $n\Delta\phi = 0 \mod 2\pi$ and ϕ determines the value of $\Delta\phi := \alpha - \beta = 2\phi + \pi \mod 2\pi$. The integer p used in the main text to find

loops on amorphous graphs that can host flat bands is found by counting how many iterations of $\Delta\phi$ are required before the phase returns to a multiple of 2π.

Numerical diagonalization of kagomé systems reveals that flat bands only exist when ϕ is a multiple of $\pi/6$. For the kagomé lattice, hexagons are the only secondary polygons and thus $6(2\phi + \pi) = 2\pi m$ for $m \in \mathbb{Z}$. This condition indeed gives that ϕ must be a multiple of $\pi/6$ to observe a flat band. Note that flat band eigenstates never occur localized around the primitive triangles of the kagomé lattice because this geometry does not lead to destructive interference when the Hamiltonian acts on such a state.

An amorphous kagomized graph, however, contains secondary polygons with $n \neq 6$ in addition to hexagons. The following condition determines the possible phases ϕ for observing flat bands in amorphous systems:

$$n\Delta\phi = n(2\phi + \pi) = 2\pi m \quad \forall m \in \mathbb{Z} \quad \text{(A4)}$$

This condition reproduces the flat bands seen in kagomé systems and predicts values of ϕ that only show flat bands in the amorphous case. An example of an amorphous-only flat band is seen at $\phi = 11\pi/10$ for $n = 5$, $m = 8$, the flat band shown in Fig. 4 in the main text.

2. Flat band degeneracy

In the previous section, we saw that flat band states are intimately connected to cycles on directed, kagomized graphs. The precise relation depends on the value of the flux ϕ. Here we will work out this relation for the case of $\phi = 0$ where one does not need to specify the direction on the graph (since the magnetic field is absent).

First, let us establish some basic properties of kagomized graphs. We consider a graph with S sites. The number of primitive triangles $N_\Delta = \frac{2}{3}S$, and, as a consequence, N_Δ is always divisible by 2 and S is always divisible by 3. The number of edges is $3N_\Delta$. Next, we would like to point out, that secondary polygons are well defined only when we consider graph's embedding. In what follows, we will assume that the graph is embedded on a torus, as has been the case for the numerical simulations in this paper. Euler's formula for the torus topology reads:

$$S - 3N_\Delta + (N_\Delta + N_{poly}) = 0, \quad \text{(A5)}$$

where N_{poly} is the number of secondary polygons in the graph. We conclude $N_{poly} = S/3$ (it would be $N_{poly} = S/3 - 1$ in the case of disk topology).

Lastly, if there are odd polygons in the graph, their number is always even. This following from the fact that the total number of edges in all polygons is given by $3N_\Delta$, and we have already established that N_Δ must be even.

From Table 1, we see that the flat band degeneracy never exceeds $S/3 + 1$. This can be interpreted as the number of independent cycles that contain an even number of vertices

(i.e. 0 or 2) of each primitive triangle. For the most part these cycles just come from secondary polygons, but we need to account for topology. We note that on a torus, the sum of cycles on all polygons vanishes, additionally, there are two non-contractible cycles. Overall, Eq. A5 gives:

$$S/3 - 1 + 2 = S/3 + 1. \qquad (A6)$$

The answer would be the same if we assumed disk topology. We expect the flat band to derive from these cycles in some way. In the rest of the section, we will perform this construction for the case $\phi = 0$.

The case of $\phi = 0$: Recall, that the Hamiltonian Eq. 1 is given by a sum of terms supported on individual primitive triangles, each of which we will refer to as a local Hamiltonian. Each term has form $|1\rangle\langle 2| + |2\rangle\langle 3| + |3\rangle\langle 1| + h.c.$ with eigenvalues $2, -1, -1$. Each flat band state has energy -2 and this is only achievable if the state lies in the -1 subspace of the local Hamiltonian for each primitive triangle, since each site is acted upon by exactly two terms.

The -1 subspace is spanned by states that have amplitudes ± 1 on the sites of any edge in the primitive triangle. Requiring that the amplitudes sum to zero on every primitive triangle leads us to conclude that the space of flat bands is equivalent to the space spanned by states supported on loops with the amplitude alternating ± 1 along the loop. We note that a loop is permitted to go over the same edge multiple times, as occurs on the edges of Dirac strings in Type-II states introduced in Sec. III. Thus, a Type-II state is also considered a loop in this construction.

Finally, we can compute the number of such states on a kagomized graph with S sites. If all secondary polygons are of even length, then the total flat band subspace spanned by the alternating states on each polygon plus the alternating states on non-contractible loops (their length can always be made even by making them use two edges of a triangle instead of one or visa versa). This is the case for periodic kagomé lattice and the number states coincides with Eq. (A6): $S/3 + 1$. In the case when there are odd secondary polygons (they must come in pairs), we built a flat band state by combining any pair polygons pairwise if adjacent (Type-I states in Sec. III) or connecting them with a Dirac string otherwise (Type-II states in Sec. III). If there are M odd secondary polygons, this procedure will yield $M - 1$ linearly independent flat band states, leading to the degeneracy of $S/3$ confirmed by numerical simulations in Table 1.

One might wonder if the Dirac strings are necessary and whether one might be able to use only non-intersecting even length loops that combine the odd secondary polygons. The graph we present in Fig. 11 gives a counter example. There are 8 flat band states: 6 come from independent even length loops and 2 are these bridged Dirac string states. Due to the pinched nature of the graph, it is impossible to connect the secondary triangles from the different petals with a loop, and one needs to use Type-II states.
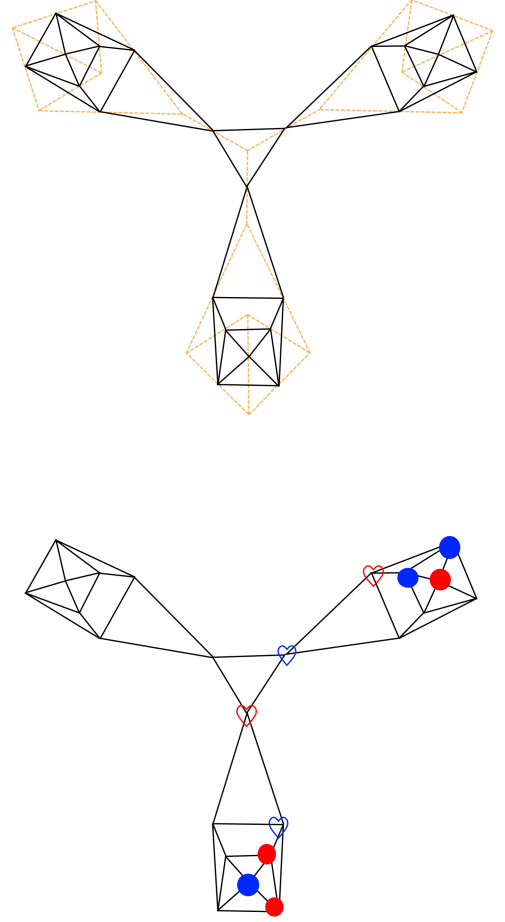

FIG. 11. Top: Voronoi (dashed orange lines) diagram and kagomization (black) of a pinched graph that necessarily hosts Type-II flat band states. Bottom: Type-II flat band state on the kagomized graph. Blue (red) circles represent un-normalized state amplitude $+1(-1)$ and blue (red) hearts denote the Dirac string that connects the two disjoint secondary triangles, with amplitudes $+2(-2)$.

Full spectrum IPR, single realization
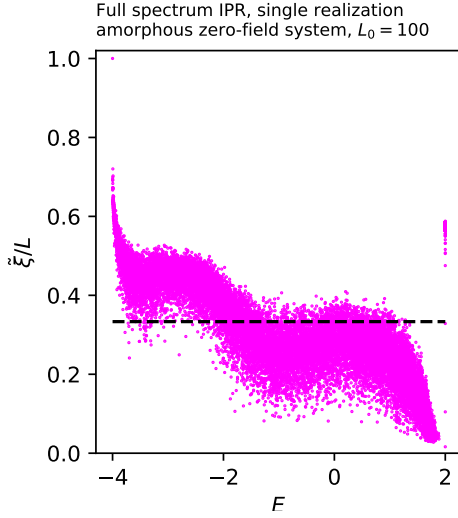amorphous zero-field system, $L_0 = 100$

FIG. 12. Scatter plot of the energy of every eigenstate of an $L_0 = 100$ system with $\phi = 0$ and its effective localization length. At $E = -4$ is a completely delocalized state and at $E = 2$ is the system flat band.

Appendix B: Localization in amorphous model in zero-field

In Supplemental Material Fig. 3, we analyze amorphous systems with $\phi = 0$, which belong to symmetry class AI. We find that states tend to localize near the upper tail of the single dispersive band. Near the fully delocalized state at $E = -4$, some states are also delocalized in character.

[1] M. Fox, *Optical properties of solids*, Vol. 3 (Oxford university press, 2010).

[2] M. Florescu, S. Torquato, and P. J. Steinhardt, Designer disordered materials with large, complete photonic band gaps, Proceedings of the National Academy of Sciences **106**, 20658 (2009).

[3] S. M. Girvin and K. Yang, *Modern condensed matter physics* (Cambridge University Press, 2019).

[4] M. Hafezi, E. A. Demler, M. D. Lukin, and J. M. Taylor, Robust optical delay lines with topological protection, Nature Physics **7**, 907–912 (2011).

[5] Z. Jia, M. Seclì, A. Avdoshkin, W. Redjem, E. Dresselhaus, J. Moore, and B. Kanté, Disorder-enhanced nonlinear topological phenomena, Science Advances **9** (2023).

[6] R. Catlow, *Defects and disorder in crystalline and amorphous solids*, Vol. 418 (Springer Science & Business Media, 2012).

[7] D. Weaire, Existence of a gap in the electronic density of states of a tetrahedrally bonded solid of arbitrary structure, Phys. Rev. Lett. **26**, 1541 (1971).

[8] M. F. Thorpe and D. Weaire, Electronic properties of an amorphous solid. ii. further aspects of the theory, Phys. Rev. B **4**, 3518 (1971).

[9] Q. Niu, D. J. Thouless, and Y.-S. Wu, Phys. Rev. B **31**, 3372 (1985).

[10] P. Torma, S. Peotta, and B. A. Bernevig, "superfluidity and quantum geometry in twisted multilayer systems", Nature Physics Reviews **4**, 528–542 (2022).

[11] J. Hu, X. Zhang, C. Hu, J. Sun, X. Wang, H. Lin, and G. Li, "correlated flat bands and quantum spin liquid state in a cluster mott insulator", Communications Physics **6** (2023).

[12] S. A. Parameswaran, R. Roy, and S. L. Sondhi, "fractional quantum hall physics in topological flat bands", Comptes Rendus Physique **14** (2013).

[13] Y. Chen, J. Huang, K. Jiang, and J. Hu, Decoding flat bands from compact localized states, Science Bulletin **68**, 3165 (2023).

[14] J. P. Wakefield, M. Kang, P. M. Neves, D. Oh, S. Fang, R. McTigue, S. Y. Frank Zhao, T. N. Lamichhane, A. Chen, S. Lee, S. Park, J.-H. Park, C. Jozwiak, A. Bostwick, E. Rotenberg, A. Rajapitamahuni, E. Vescovo, J. L. McChesney, D. Graf, J. C. Palmstrom, T. Suzuki, M. Li, R. Comin, and J. G. Checkelsky, Three-dimensional flat bands in pyrochlore metal cani2, Nature **623**, 301 (2023).

[15] E. J. BERGHOLTZ and Z. LIU, Topological flat band models and fractional chern insulators, International Journal of Modern Physics B **27**, 1330017 (2013), https://doi.org/10.1142/S021797921330017X.

[16] P. W. Anderson, Absence of diffusion in certain random lattices, Phys. Rev. **109**, 1492 (1958).

[17] K. Efetov, *Supersymmetry in disorder and chaos* (Cambridge university press, 1999).

[18] F. Evers and A. D. Mirlin, Anderson transitions, Rev. Mod. Phys. **80**, 1355 (2008).

[19] M. Puschmann, Anderson transitions on random Voronoi-Delaunay lattices, PhD thesis (2017).

[20] Q. Marsal, D. Varjas, and A. Grushin, Topological weaire–thorpe models of amorphous matter, Proc. National Academy of Science **117** (2020).

[21] M. Puschmann, P. Cain, M. Schreiber, and T. Vojta, Multifractal analysis of electronic states on random Voronoi-Delaunay lattices, Eur. Journal Phys. B **88** (2015).

[22] U. Grimm, R. A. Romer, and G. Schliecker, Electronic states in topologically disordered systems, Annals of Physics **7**, 389 (1998).

[23] D. Logan and P. Wolynes, Dephasing and Anderson localization in topologically disordered systems, Phys. Rev. B **36** (1987).

[24] A. Altland and M. Zirnbauer, Nonstandard symmetry classes in mesoscopic normal-superconducting hybrid structures, Phys. Rev. B **55**, 1142 (1997).

[25] N. Mitchell, L. M. Nash, D. Hexner, A. Turner, and W. T. M. Irvine, Amorphous topological insulators constructed from random point sets, Nature Physics **14**, 380 (2018).

[26] M. B. Dillencourt, Realizability of delaunay triangulations, Information Processing Letters **33**, 283 (1990).

[27] N. Matsumoto, A. Nakamoto, and S. Negami, Diagonal flips in plane graphs with triangular and quadrangular faces, Discrete Applied Mathematics **283**, 292 (2020).

[28] S. Negami, Diagonal flips in triangulations of surfaces, Discrete Mathematics **135**, 225 (1994).

[29] O. Aichholzer, T. Hackl, D. Orden, A. Pilz, M. Saumell, and B. Vogtenhuber, Flips in combinatorial pointed pseudo-triangulations with face degree at most four, International Journal of Computational Geometry I& Applications **24**, 197 (2014).

[30] L. Chen, T. Mazaheri, A. Seidel, and X. Tang, The impossibility of exactly flat non-trivial Chern bands in strictly local periodic tight binding models, J. Phys. A: Math. and Theor. **47**, 152001 (2014).

[31] P. M. Neves, J. P. Wakefield, S. Fang, H. Nguyen, L. Ye, and J. G. Checkelsky, Crystal net catalog of model flat band materials, npj Computational Materials **10**, 39 (2024).

[32] N. F. Mott and R. S. Allgaier, Localized states in disordered lattices, Physica Status Solidi B **21**, 343 (1967).

[33] A. MacKinnon and B. Kramer, One-Parameter Scaling of Localization Length and Conductance in Disordered Systems, Phys. Rev. Lett. **47** (1981).

[34] B. I. Shklovskii, B. Shapiro, B. R. Sears, P. Lambrianides, and H. Shore, Statistics of spectra of disordered systems near the metal-insulator transition, Phys. Rev. B **47**, 11487 (1993).

[35] B. Bulka, B. Kramer, and A. MacKinnon, Mobility Edge in the Three Dimensional Anderson Model, Z. Phys. B **60**, 13 (1985).

[36] T. Guhr, A. Muller-Groeling, and H. A. Weidenmuller, Random-matrix theories in quantum physics: common concepts, Physics Reports **299** (1998).

[37] M. Zirnbauer, Symmetry Classes, arXiv preprint arXiv:1001.0722 (2010).

[38] A. W. W. Ludwig, M. P. A. Fisher, R. Shankar, and G. Grinstein, Integer quantum Hall transition: An alternative approach and exact results, Phys. Rev. B **50**, 7526 (1994).

[39] B. Huckestein, Scaling theory of the integer quantum Hall effect, Rev. Mod. Phys. **67**, 357 (1995).

[40] B. Sbierski, E. J. Dresselhaus, J. E. Moore, and I. A. Gruzberg, Criticality of two-dimensional disordered Dirac fermions in the unitary class and universality of the integer quantum Hall transition, Phys. Rev. Lett **126**, 076801 (2021).

[41] D. L. Bergman, C. Wu, and L. Balents, Band touching from real space topology in frustrated hopping models, Phys. Rev. B **78**, 357 (2008).

[42] S. Kim, A. Agarwala, and D. Chowdhury, Fractionalization and Topology in Amorphous Electronic Solids, Phys. Rev. Lett. **130** (2023).

[43] G. Cassella, P. P. D'Ornellas, T. Hodson, W. M. H. Natori, and J. Knolle, An Exact Chiral Amorphous Spin Liquid, arXiv preprint arXiv:2208.08246v2 (2022).

[44] T. Wang, Z. Pan, T. Ohtsuki, I. A. Gruzberg, and R. Shindou, Multicriticality of Two-dimensional Class D Disordered Topological Superconductors, Phys. Rev. B **104**, 014206 (2021).

[45] T. Senthil and M. P. A. Fisher, Quasiparticle localization in superconductors with spin-orbit scattering, Phys. Rev. B **61**, 9690 (2000).

[46] M. N. Ivaki, I. Sahlberg, and T. Ojanen, Criticality in amorphous topological matter: Beyond the universal scaling paradigm, Phys. Rev. Research **2** (2020).